

## Failure Analysis of Three $\text{Si}_3\text{N}_4$ Balls

1 December 2001

Prepared by

M. J. O'BRIEN  
Space Materials Laboratory  
Laboratory Operations

N. PRESSER  
Electronics and Photonics Laboratory  
Laboratory Operations

Prepared for

SPACE AND MISSILE SYSTEMS CENTER  
AIR FORCE SPACE COMMAND  
2430 E. El Segundo Boulevard  
Los Angeles Air Force Base, CA 90245

Engineering and Technology Group

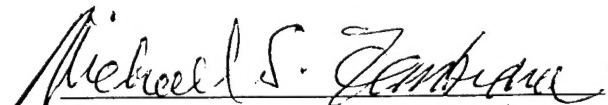
APPROVED FOR PUBLIC RELEASE;  
DISTRIBUTION UNLIMITED

20020118 244

This report was submitted by The Aerospace Corporation, El Segundo, CA 90245-4691, under Contract No. F04701-00-C-0009 with the Space and Missile Systems Center, 2430 E. El Segundo Blvd., Los Angeles Air Force Base, CA 90245. It was reviewed and approved for The Aerospace Corporation by P. D. Fleischauer, Principal Director, Space Materials Laboratory; and B. Jadusziwer, Principal Director, Electronics and Photonics Laboratory. Michael Zambrana was the project officer for the Mission-Oriented Investigation and Experimentation (MOIE) program.

This report has been reviewed by the Public Affairs Office (PAS) and is releasable to the National Technical Information Service (NTIS). At NTIS, it will be available to the general public, including foreign nationals.

This technical report has been reviewed and is approved for publication. Publication of this report does not constitute Air Force approval of the report's findings or conclusions. It is published only for the exchange and stimulation of ideas.



Michael Zambrana  
SMC/AXE

# REPORT DOCUMENTATION PAGE

Form Approved  
OMB No. 0704-0188

Public reporting burden for this collection of information is estimated to average 1 hour per response, including the time for reviewing instructions, searching existing data sources, gathering and maintaining the data needed, and completing and reviewing this collection of information. Send comments regarding this burden estimate or any other aspect of this collection of information, including suggestions for reducing this burden to Department of Defense, Washington Headquarters Services, Directorate for Information Operations and Reports (0704-0188), 1215 Jefferson Davis Highway, Suite 1204, Arlington, VA 22202-4302. Respondents should be aware that notwithstanding any other provision of law, no person shall be subject to any penalty for failing to comply with a collection of information if it does not display a currently valid OMB control number. PLEASE DO NOT RETURN YOUR FORM TO THE ABOVE ADDRESS.

1. REPORT DATE (DD-MM-YYYY) 01-12-2001		2. REPORT TYPE Failure Analysis of Three Si <sub>3</sub> N <sub>4</sub> Balls		3. DATES COVERED (From - To)	
4. TITLE AND SUBTITLE				5a. CONTRACT NUMBER F04701-00-C-0009	
				5b. GRANT NUMBER	
				5c. PROGRAM ELEMENT NUMBER	
6. AUTHOR(S)  M. J. O'Brien and N. Presser				5d. PROJECT NUMBER	
				5e. TASK NUMBER	
				5f. WORK UNIT NUMBER	
7. PERFORMING ORGANIZATION NAME(S) AND ADDRESS(ES)  The Aerospace Corporation Laboratory Operations El Segundo, CA 90245-4691				8. PERFORMING ORGANIZATION REPORT NUMBER  TR-2001(8565)-1	
9. SPONSORING / MONITORING AGENCY NAME(S) AND ADDRESS(ES)  Space and Missile Systems Center Air Force Space Command 2430 E. El Segundo Blvd. Los Angeles Air Force Base, CA 90245				10. SPONSOR/MONITOR'S ACRONYM(S) SMC	
				11. SPONSOR/MONITOR'S REPORT NUMBER(S) SMC-TR-02-07	
12. DISTRIBUTION/AVAILABILITY STATEMENT  Approved for public release; distribution unlimited.					
13. SUPPLEMENTARY NOTES					
14. ABSTRACT  A test series was undertaken to demonstrate the rolling-element fatigue life and Weibull distribution of advanced material bearings compared with conventional 52100 steel bearings. The candidate advanced material bearing consisted of Norton Si <sub>3</sub> N <sub>4</sub> NBD-200 balls and Rex 20 steel races. In general, the advanced material bearings demonstrated much greater lives than the conventional bearings.  A fractographic analysis of three failed ceramic balls from the test series was performed in an attempt to assign a cause for the failures. In all three cases, the initiation of the final fracture was traced back to a relatively small initiation site. In two cases, interesting features were identified that may represent the potential cause for the failure. These potential causes may represent small manufacturing defects that might be sintering voids with diameters of less than 2 µm. It is possible, however, that such small defects should not be considered manufacturing defects but should instead be considered defects inherent to the material. In the third case, no distinctive features were identified in the small initiation site, and no potential cause was identified.  The balls failed after very long tests under intentionally elevated loading, which raised the Hertzian contact stresses. This suggests that the identified potential causes were, in the worst case, possible manufacturing flaws of very small size and very little apparent consequence, in practice. That is, the balls' very long lives under elevated loading suggest that the manufacturer is controlling the population of pre-existing manufacturing flaws very well.					
15. SUBJECT TERMS Ceramic, silicon nitride, Si <sub>3</sub> N <sub>4</sub> , hybrid bearing, failure analysis, electron fractography, ball, rolling element fatigue, Hertzian contact, sintering void, Weibull distribution.					
16. SECURITY CLASSIFICATION OF:  UNCLASSIFIED			17. LIMITATION OF ABSTRACT  UNCLASSIFIED	18. NUMBER OF PAGES  18	19a. NAME OF RESPONSIBLE PERSON Michael O'Brien
a. REPORT UNCLASSIFIED	b. ABSTRACT UNCLASSIFIED	c. THIS PAGE UNCLASSIFIED			19b. TELEPHONE NUMBER (include area code) (310)336-2878

## Contents

1. Background .....	1
2. Testing of Candidate Advanced Material Consisting of Norton Si <sub>3</sub> N <sub>4</sub> Balls and Rex 20 Steel Races .....	3
3. Summary .....	5
4. Observations .....	7
4.1 Ball U828-802 #21 (1548 hours of service until failure).....	7
4.2 Ball U828-802 #2 (slightly greater than 3400 hours of service until failure).....	9
4.3 Ball U828-802 #7 (slightly greater than 3400 hours of service until failure).....	15
References.....	19

## 1. Background

A test series was undertaken to demonstrate the rolling-element fatigue life of advanced material bearings compared with conventional 52100 steel bearings.<sup>1,2</sup> Fatigue testing was performed using a standard fatigue test fixture. Six sets of four bearings (207 size) were tested for each candidate material using the first-in-four technique to obtain a Weibull distribution. All candidate bearings were run at 5400 rpm and lubricated with a continuous flow of MIL-L-7808 oil at 2 pints/min/bearing. The oil was maintained at a temperature of 160°F and filtered to the 3- $\mu$ m level. The test system was capable of detecting a spall as small 1/8-in.-dia on the 15/32-in.-dia balls tested.

Test protocol was sudden-death statistics using multiple test groups of four bearings each. The first failure in the group of four bearings suspended the other three bearings, resulting in an estimate of the  $L_{15.91}$  life. The failure lifetimes and statistical comparisons are addressed in Aerospace Technical Report ATR-2000(8260)-2, 2 April 2000, where a provisional design chart for these bearings is presented.

## **2. Testing of Candidate Advanced Material Consisting of Norton Si<sub>3</sub>N<sub>4</sub> Balls and Rex 20 Steel Races**

To provide a reference, standard steel bearings with 52100 steel balls and races were tested. The axial load was 3000 lb-f, which was equivalent to a mean Hertzian stress of 272 kpsi. For the six sets of four bearings tested, the times to first failure in each set were 17, 47, 127, 339, 364, and 910 h.

The candidate advanced material bearing consisted of Norton Si<sub>3</sub>N<sub>4</sub> NBD-200 balls and Rex 20 steel races. To provide equivalent contact stress, the axial load was 1500 lb-f, which gave the same mean Hertzian stress of 272 kpsi used to test the standard 52100 steel bearing. When all six tests were discontinued upon reaching the maximum target life, none of the six sets showed a single failure. Specifically, the six tests ran for 2630, 2784, 2630, 2611, 2611, and 2611 h when testing was ended (again, without any recorded failures).

The Rex 20/Si<sub>3</sub>N<sub>4</sub> hybrid bearings substantially outperformed 52100 steel bearings at equivalent stress. To learn how they would perform at equivalent axial loads, an additional series of tests was run for the Rex 20/Si<sub>3</sub>N<sub>4</sub> bearings at an axial load of 3000 lb-f, which was the same load used for the 52100 bearings. Because of the higher moduli of Rex 20 and Si<sub>3</sub>N<sub>4</sub>, the Hertzian stresses are substantially higher for these hybrid bearings (332 kpsi) than for the 52100 steel bearings (272 kpsi) under this identical axial load of 3000 lb-f.

Due to limited availability of Rex 20 races, only four sets of four bearings were tested under this condition of equivalent axial load. Of the four resulting failures, three were ball failures (at 1548, 3408, and 3441 h). The fourth failure was a steel race failure (at 2250 h). Specifically, the ball labeled "U828-802 #21" failed at 1548 h. The two balls labeled "U828-802 #2" and "U828-802 #7" represented the other two failures (3408 and 3441 h), although our records don't indicate which of the two was which.

### 3. Summary

A fractographic analysis of the three failed balls (U828-802 #2, #7, #21) was performed in an attempt to assign a cause for the failures. In all three cases, the initiation of the final fracture was traced back to a relatively small initiation site. In two cases (#2 and #7), interesting features were identified that may represent the potential cause for the failure. These potential causes may represent small manufacturing defects that might be sintering voids with diameters of less than 2  $\mu\text{m}$ . It is possible, however, that such small defects should not be considered manufacturing defects but should instead be considered defects inherent to the material. In the third case (#21), no distinctive features were identified in the small initiation site, and no potential cause was identified.

Balls #2 and #7, for which potential causes were identified, failed after very long tests of more than 3400 h under elevated loading, which raised the Hertzian contact stresses. This suggests that the identified potential causes were, in the worst case, possible manufacturing flaws of very small size and very little apparent consequence, in practice. That is, the balls' very long lives under elevated loading suggest that the manufacturer is controlling the population of pre-existing manufacturing flaws very well. On the other hand, the fractography of ceramic balls is sparsely documented. It would be useful to develop a larger library of fractographic analyses in order to understand the true significance of the features identified here and to provide a context for these failures.

The three failed balls have been returned to the manufacturer so that they can also analyze the failures.

## 4. Observations

As an explanatory note, Wallner lines are curved and wavelike markings on the surface of fractured ceramic. The fracture origin is always on the concave side of the Wallner lines, which can be used to determine the origin and direction of propagation of the fracture. As terminology, the fracture origin is “upstream” in the fracture, and the fracture grows in the direction from the “upstream” location to the “downstream” location.

### 4.1 Ball U828-802 #21 (1548 hours of service until failure)

Figure 1 is a low-magnification view of the entire spall from a perspective perpendicular to the spall. The circular Wallner lines seem to radiate on the left and right from an initiation site labeled “A,” with the concave sides of the Wallner lines pointing back towards this initiation site. The site labeled “A” is a broad, flat “plateau.”

Figure 2 is another low-magnification view centered on site “A” showing the neighboring Wallner lines more distinctly. Figure 3 is a slightly higher magnification view at 50x centered to the right-hand side of the site “A” and Figure 4 is a companion view at 20x centered to the left-hand side of the site “A.” Figures 3 and 4 are taken at oblique angles to highlight the concave Wallner lines, which again point back towards the site “A,” which is therefore identified as the initiation site.

Figures 5, 6, and 7 are a series (at magnifications of 110x, 100x, and 100x) centered on the site “A.” Figure 5 is from an orthogonal perspective, and Figures 6 and 7 from oblique perspectives. The circular Wallner lines seen in site “A” form a “bull’s eye” pattern around a central point, labeled “B,” which is within the region labeled “A” and approximately in its center. The pattern of Wallner lines implies that site “B” is the upstream location where failure initiated.

Figures 8 and 9 are views at 200x and 250x centered at site “B.” Detailed inspection of site “B” at still higher magnifications did not seem to reveal a clear cause for the initiation of the fracture on site “B.”

---

\* “The wavelike contour is caused by temporary excursion of the crack front out of plane in response to a tilt in the axis of principal tension caused by an elastic pulse. The Wallner line is the locus of interception of the spreading pulse with successive points along the running crack front,” from *Engineered Materials Handbook Volume 4, Ceramics and Glasses*, S. J. Schneider, volume chairman, ASM International, Metals Park, OH, pp. 634.



Fig 1



Fig 2

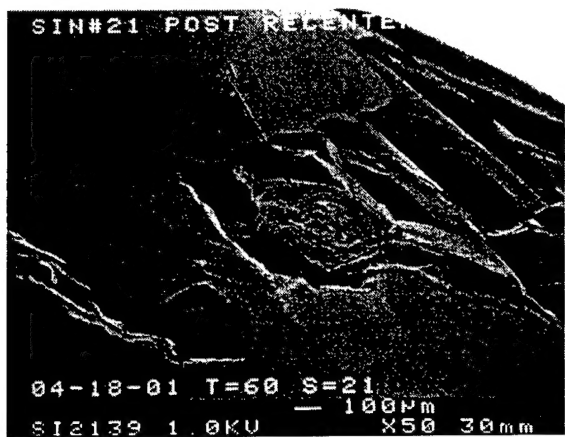


Fig 3



Fig 4 (this view is upside down from the view in Fig 1)

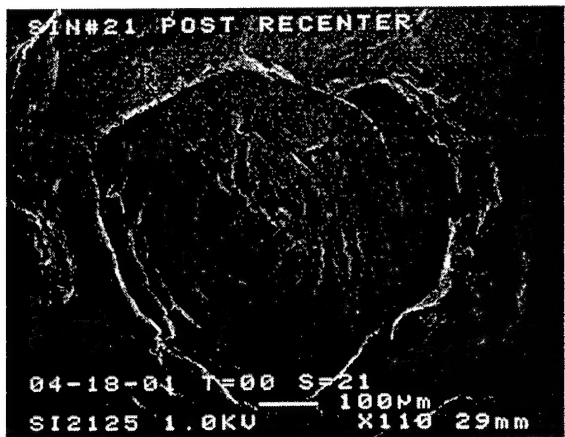


Fig 5



Fig 6

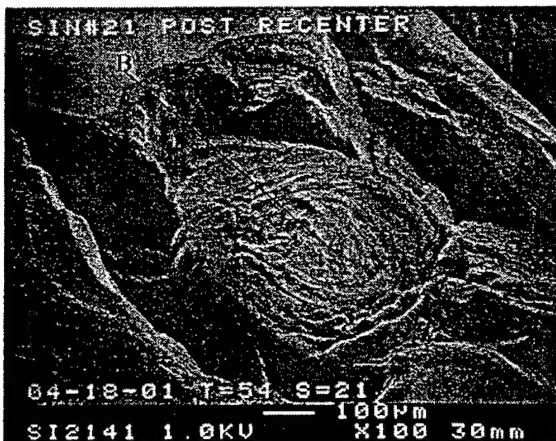


Fig 7

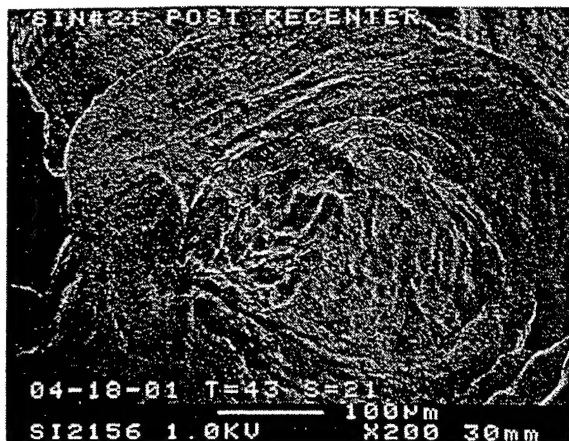


Fig 8

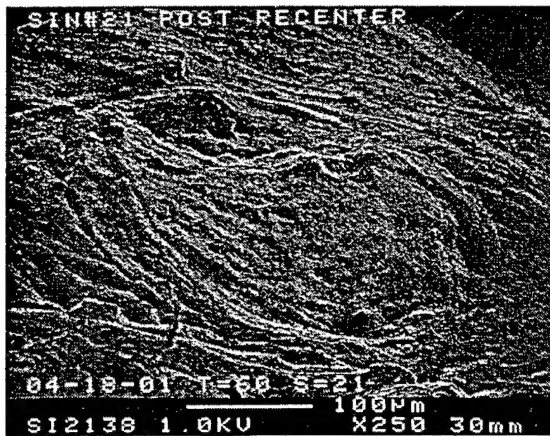


Fig 9

#### 4.2 Ball U828-802 #2 (slightly greater than 3400 hours of service until failure)

Figure 10 is a low-magnification view of the entire spall from a perspective orthogonal to the spall. The circular Wallner lines are evident in the upper and middle parts of the spall, and the concave lines seem to radiate back to a point in the lower part of the spall. To orient the discussion of subsequent fractographs that show finer detail, four features are labeled in Figure 10. Feature "A" is a region of Wallner lines in the middle of the spall. Feature "B" is a region of Wallner lines in the lower part of the spall. Feature "C" is a void in a triangular pocket defined by the intersection of three cracks. The long diagonal line labeled "D" is a deep "trench-like" fracture that is not obvious from this perspective.

Figure 11 is a low-magnification oblique view showing better the Wallner lines in the upper region of the spall. Features "A" and "B," which are the regions of Wallner lines, are labeled and reinforce the observation that the upstream location of the fracture initiation is in the lower part of the spall with the middle and upper parts of the spall downstream from the initiation site. The location of the void



Fig 10.

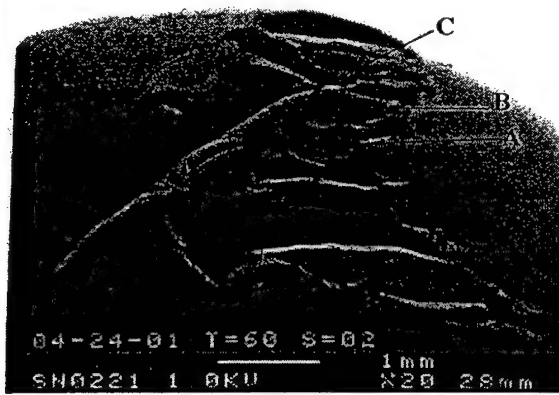


Fig 11

is labeled "C," although the triangular pocket is not obvious in this view. The long and deep fracture, labeled "D," is more obvious in this view. An interesting feature, labeled "E," is a patch of virgin surface that did not spall away.

Figures 12, 13, and 14 are low-magnification views taken by successively rotating the line of sight. The concavity of the regions of Wallner lines, labeled "A" and "B," again reinforce that fracture initiation occurred in the lower part of the spall. The location of the void, labeled "C," is labeled in the lower part of the spall. The deep fracture, labeled "D," is seen to intersect the void. Actually, these three views cumulatively show that three separate fractures intersect at the void. To provide a landmark, the location of the unspalled virgin surface is labeled "E."

Figures 15 and 16 are orthogonal views of the lower part of the spall at higher magnifications. The Wallner lines, labeled "A" and "B," show that fracture initiated between region "B" and the lower-most part of the spall. That is, region "A" is downstream of region "B," which, in turn, is downstream of the site of fracture initiation. Void "C" is located in this area upstream of the region "B" and is considered a possible candidate responsible for initiation of the spall. The deep crack, "D", radiates from the void, as do two other cracks, labeled "F" and "G".

Figure 17 is a higher magnification orthogonal view of the middle and upper parts of the spall. The Wallner lines labeled "A" are visible, although the other region of Wallner lines, "B," is just beneath the lower edge of the frame and is not visible. Again, the concave sides of the Wallner lines point upstream to the site in the lower part of the spall where fracture initiated.

Figure 18 is an oblique view taken from a line of sight from the upper part of the spall. The Wallner lines, "A" and "B," are labeled. The void, "C," is not visible, but its location is labeled. The three cracks, "D", "F," and "G," are seen to be radiating from the location of the void. As a landmark, the unspalled spot of virgin surface is labeled "E".



Fig 12



Fig 13



Fig 14



Fig 15

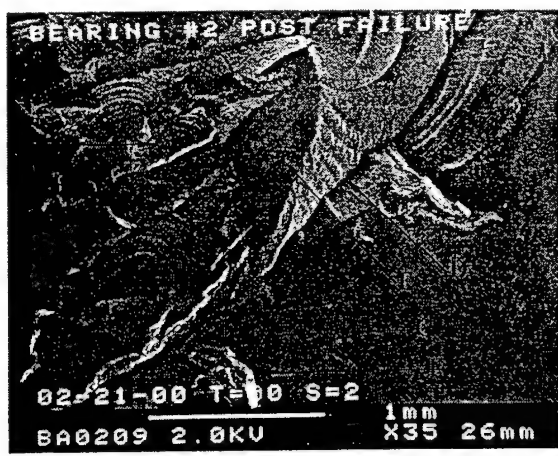


Fig 16



Fig 17

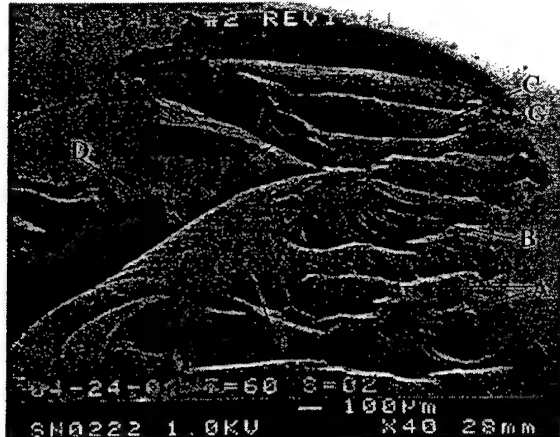


Fig 18

Figure 19 is an oblique view of the middle part of the spall whose line of sight is rotated from the line of sight used in Figure 18. The Wallner lines, "A" and "B," and the unspalled spot, "E," are labeled. The deep crack, "D," is seen running diagonally across the back of the fractograph.

Figures 20, 21, 22, 23, 24, 25, and 26 are progressively higher magnification views (at 25x, 60x, 180x, 550x, 1400x, 3500x, and 10,000x, respectively) from an orthogonal perspective and centered on the void, "C," which is at the junction of the three cracks, "D," "F," and "G." Figure 27 is a view of the void at 1500x from a different perspective that "sights" down the bore of the void. Figure 28 is a view at an intermediate magnification of 5000x from still another perspective. Figure 29 is a micrograph at a slightly higher accelerating voltage, 3 kV, that shows that the region immediately around the void charges, although material further away does not.



Fig 19

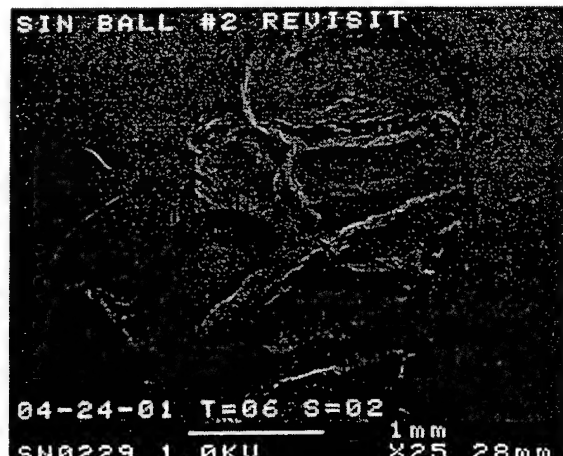


Fig 20



Fig 21



Fig 22



Fig 23

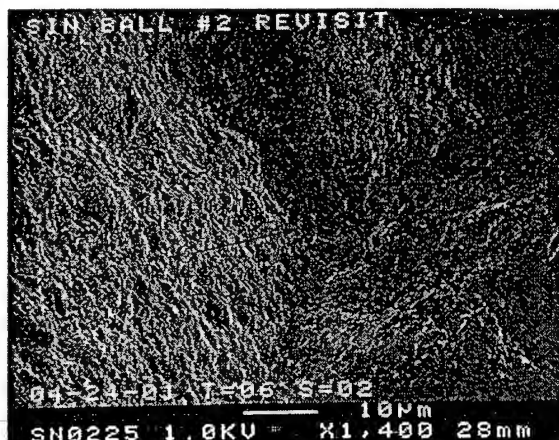


Fig 24

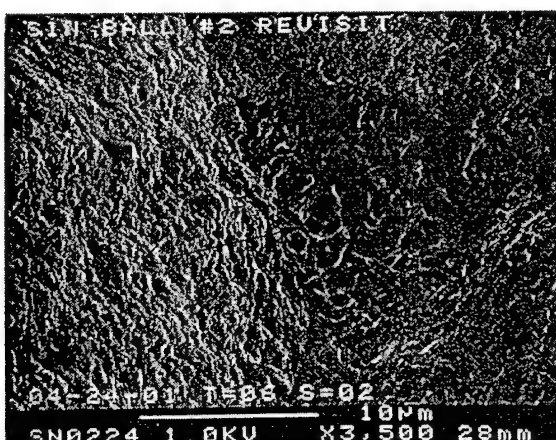


Fig 25

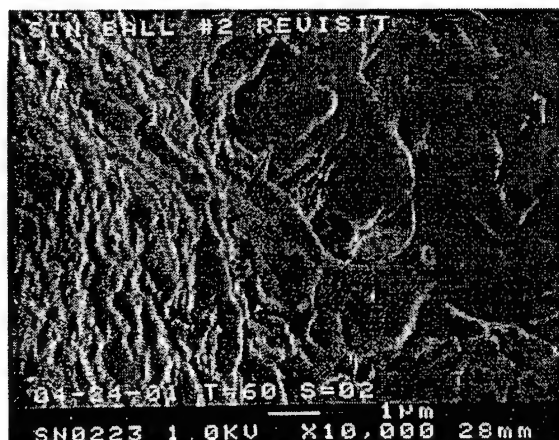


Fig 26

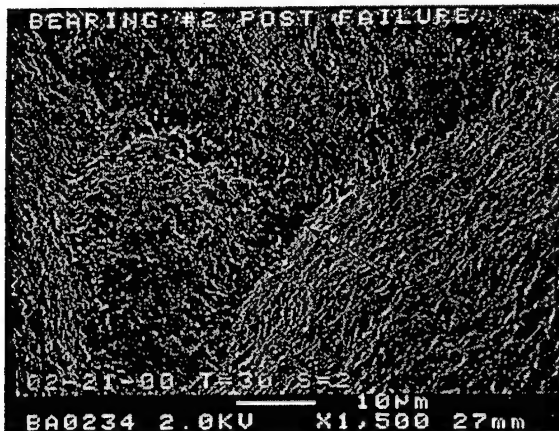


Fig 27

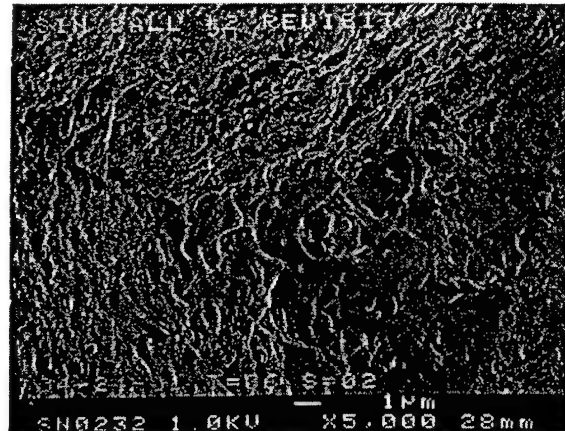


Fig 28

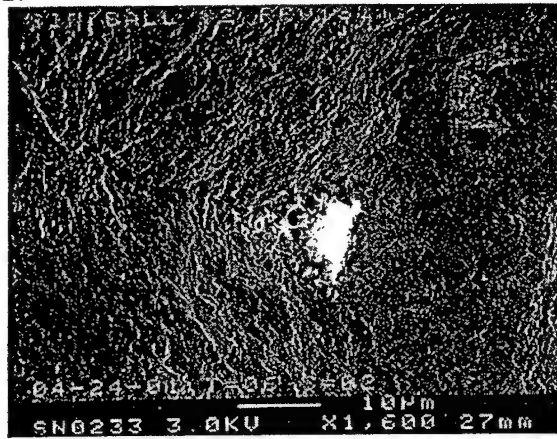


Fig 29

The void, which is approximately 2  $\mu\text{m}$  in diameter, sits in a triangular region whose appearance differs from the fracture surface around it, which is seen most clearly in Figures 25, 26, and 28. This change in appearance may imply that the triangular region is not the same chemistry as the material around it. For example, the region may be a pocket of segregated glassy material at the triple junction between adjacent grains of crystalline  $\text{Si}_3\text{N}_4$ . The observation that the triangular region charges implies that the region has a higher electrical resistivity than the material around it. A higher electrical resistivity is consistent with a pocket of glassy material rich in the sintering aids used in this  $\text{Si}_3\text{N}_4$ . The glassy sintering aids might be expected to be more insulative than the bulk  $\text{Si}_3\text{N}_4$  ceramic.

Alternatively, the change in appearance might imply that the triangular region possessed a different history than the material around it during the fracture process. For example, if the void does happen to represent the initiation of the spall, then the region may be the site where a sub-critical pre-crack developed and slowly grew by fatigue over several million Hertzian loading cycles until it reached the critical size at which the rest of the spall fractured. During the course of the fatigue cycles, asperities may have been smoothed away as the opposing faces of the pre-crack opened and closed, giving the change in appearance compared to the larger fracture surface around it.

It is uncertain, however, whether the void represented the initiation site for the fracture, whether the void developed as damage late in the fracture, or whether the void was unrelated to the fracture. If the void was responsible for fracture initiation, it may be a small sintering pore where the ceramic did not fully densify.

#### 4.3 Ball U828-802 #7 (slightly greater than 3400 hours of service until failure)

Figures 30, 31, and 32 are low-magnification views of the entire spall. The circular Wallner lines seem to radiate from a failure that originated in a broad, flat "plateau." The Wallner lines radiate down several "stepped" regions, with the concave sides of the Wallner lines pointing back towards the plateau from which the failure seems to have initiated. The concavity reinforces the notion that the plateau is "upstream" in the fracture, and the several stepped regions are "downstream." The feature "C" is labeled in Figure 32 but explained later in this discussion.

Figures 33, 34, and 35 are higher magnification views of the plateau from which fracture is believed to have initiated. The Wallner lines form a "bull's eye" pattern around a central point. The "thumb-



Fig 30

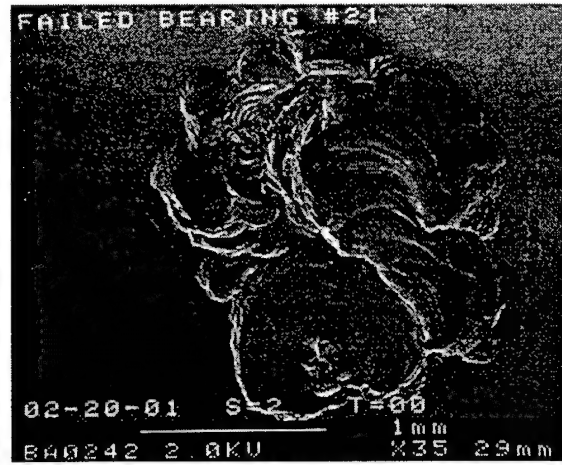


Fig 31 (the view is upside down from the previous figure)

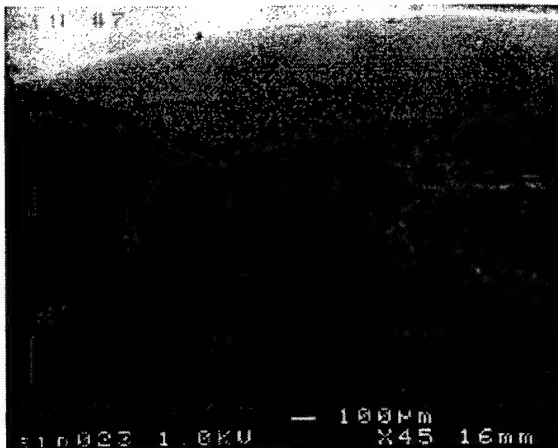


Fig 32

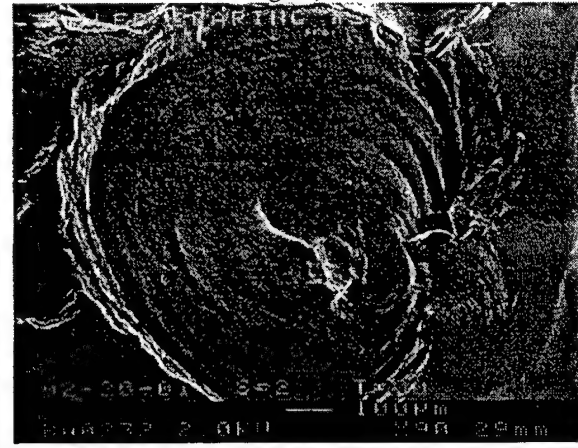


Fig 33

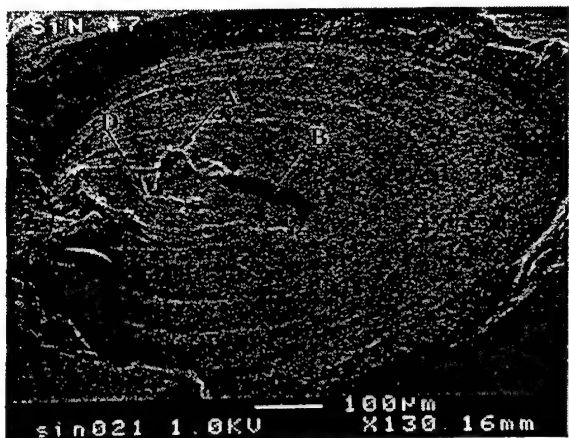


Fig 34

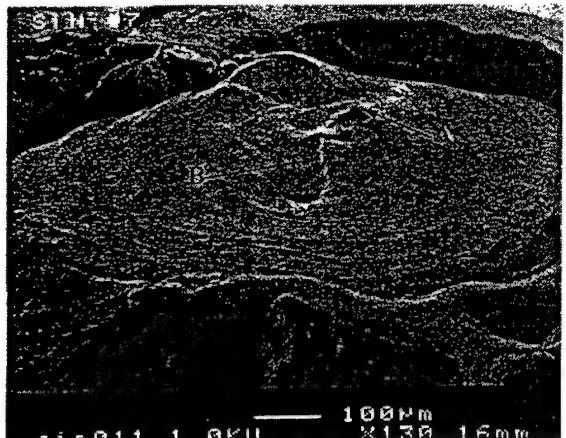


Fig 35

shaped" feature labeled "A" is a landmark used to orient subsequent discussion. Running off from point "A" is a crack-like feature labeled "B," which changes slightly in Figure 33. Another landmark is labeled "D."

Figures 36, 37, 38, 39, and 40 are progressively higher magnification views (at 95x, 300x, 1500x, 3500x and 15,000x, respectively) of a separate crack-like feature, labeled "E," from an orthogonal perspective. Feature "E" is at the base of feature "A" near feature "D." Feature "A" is labeled in Figures 36, 37, and 38 for orientation. The feature "E" is just inboard of the tightly spaced Wallner lines in the upper right hand corner of Figure 37, which reinforces the notion that feature "E" is in the right location to be the site for fracture initiation.

Figures 39 and 40 show an interesting feature in the crack-like feature "E." Ligaments span the crack-like feature. The ligaments have a distinctive elliptical shape that might be characteristic of the neck that forms during sintering and pore consolidation. The neck's elliptical shape might be interpreted as the negative radius of curvature that forms at the junction between two sintered particles. That is, the ligaments may be the remnants of a string of small sintering voids that did not fully densify. If so, then the ligaments might be expected to be glassy pockets rich in the liquid-phase sintering aids used in this ceramic. It is uncertain, however, whether the ligaments represented the initiation site for the fracture, whether the ligaments developed as damage late in the fracture, or whether the ligaments were unrelated to the fracture.

An interesting "star burst" pattern, labeled "C," is visible in Figures 32, 36, 41, and 42. The high-magnification view in Figure 42 shows several cracks radiating from a central "pit." It is uncertain whether the star burst represents the fracture initiation or whether it occurred early or late in the fracture.

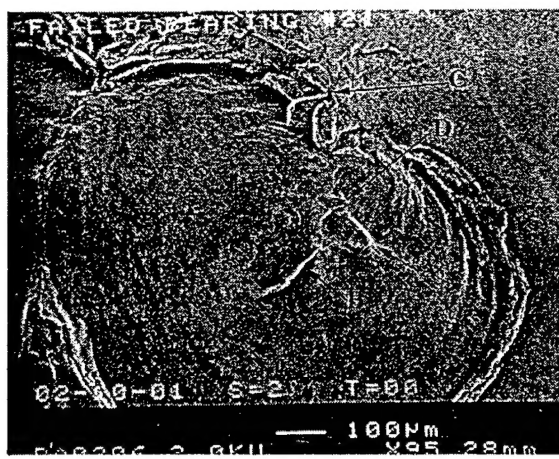


Fig 36

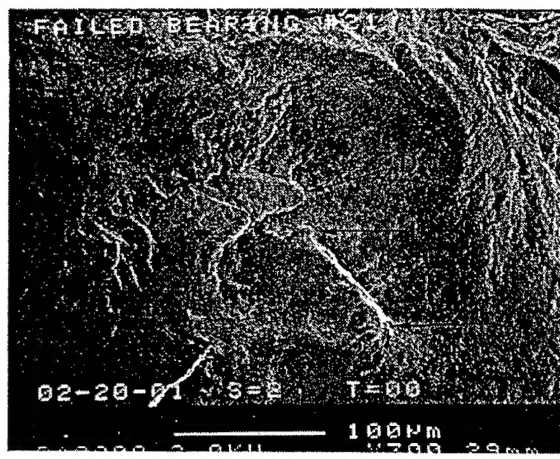


Fig 37

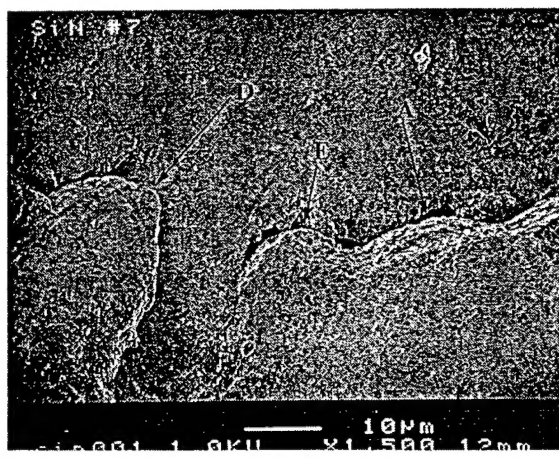


Fig 38

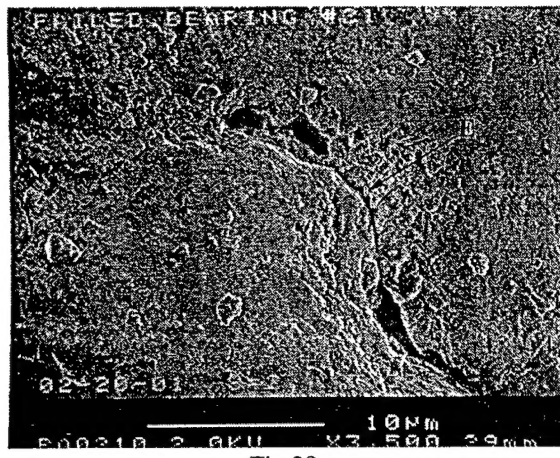


Fig 39

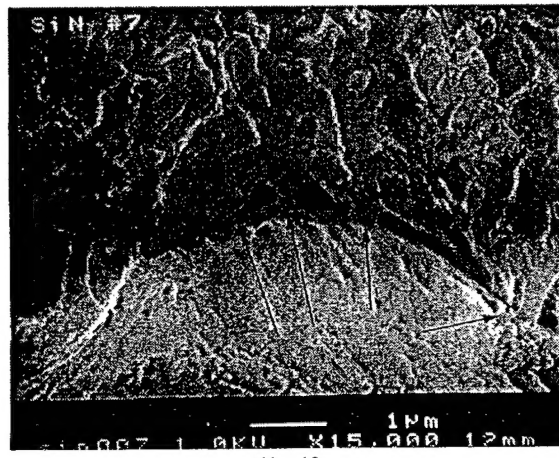


Fig 40

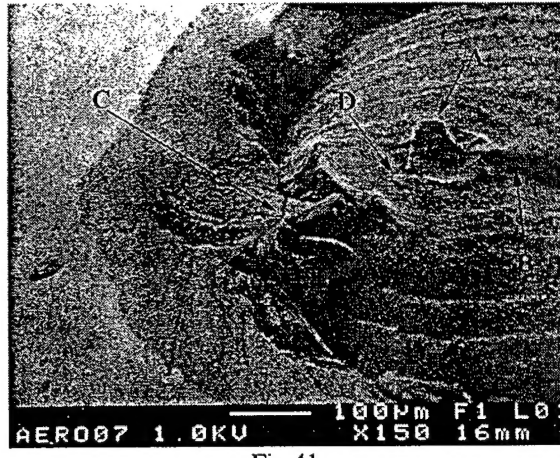


Fig 41

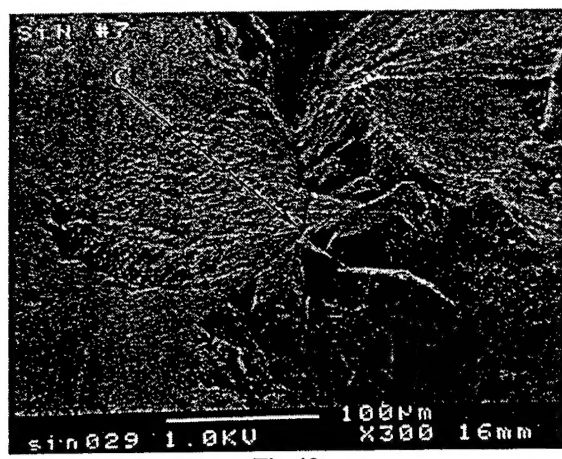


Fig 42

## References

1. W. Park et al., "Rolling Contact Fatigue and Load Capacity Tests of M62 Bearing Steel," *32<sup>nd</sup> Aerospace Mechanisms Symposium Proceedings*, S. W. Walker (ed.), Cocoa Beach, FL, May 13–15, 1998 pp. 237–251.
2. W. Park et al., "Microstructure, Fatigue Life and Load Capacity of PM Tool Steel REX20 for Bearing Applications," *Lubrication Engineering*, June 1999, pp. 20–30.

## LABORATORY OPERATIONS

The Aerospace Corporation functions as an "architect-engineer" for national security programs, specializing in advanced military space systems. The Corporation's Laboratory Operations supports the effective and timely development and operation of national security systems through scientific research and the application of advanced technology. Vital to the success of the Corporation is the technical staff's wide-ranging expertise and its ability to stay abreast of new technological developments and program support issues associated with rapidly evolving space systems. Contributing capabilities are provided by these individual organizations:

**Electronics and Photonics Laboratory:** Microelectronics, VLSI reliability, failure analysis, solid-state device physics, compound semiconductors, radiation effects, infrared and CCD detector devices, data storage and display technologies; lasers and electro-optics, solid state laser design, micro-optics, optical communications, and fiber optic sensors; atomic frequency standards, applied laser spectroscopy, laser chemistry, atmospheric propagation and beam control, LIDAR/LADAR remote sensing; solar cell and array testing and evaluation, battery electrochemistry, battery testing and evaluation.

**Space Materials Laboratory:** Evaluation and characterizations of new materials and processing techniques: metals, alloys, ceramics, polymers, thin films, and composites; development of advanced deposition processes; nondestructive evaluation, component failure analysis and reliability; structural mechanics, fracture mechanics, and stress corrosion; analysis and evaluation of materials at cryogenic and elevated temperatures; launch vehicle fluid mechanics, heat transfer and flight dynamics; aerothermodynamics; chemical and electric propulsion; environmental chemistry; combustion processes; space environment effects on materials, hardening and vulnerability assessment; contamination, thermal and structural control; lubrication and surface phenomena.

**Space Science Applications Laboratory:** Magnetospheric, auroral and cosmic ray physics, wave-particle interactions, magnetospheric plasma waves; atmospheric and ionospheric physics, density and composition of the upper atmosphere, remote sensing using atmospheric radiation; solar physics, infrared astronomy, infrared signature analysis; infrared surveillance, imaging, remote sensing, and hyperspectral imaging; effects of solar activity, magnetic storms and nuclear explosions on the Earth's atmosphere, ionosphere and magnetosphere; effects of electromagnetic and particulate radiations on space systems; space instrumentation, design fabrication and test; environmental chemistry, trace detection; atmospheric chemical reactions, atmospheric optics, light scattering, state-specific chemical reactions and radiative signatures of missile plumes.

**Center for Microtechnology:** Microelectromechanical systems (MEMS) for space applications; assessment of microtechnology space applications; laser micromachining; laser-surface physical and chemical interactions; micropulsion; micro- and nanosatellite mission analysis; intelligent microinstruments for monitoring space and launch system environments.

**Office of Spectral Applications:** Multispectral and hyperspectral sensor development; data analysis and algorithm development; applications of multispectral and hyperspectral imagery to defense, civil space, commercial, and environmental missions.